Proceedings of China-Japan Joint Conference on Hydraulic Machinery and Equipment
Hangzou, China, October 8-11, 1984

DYNAMIC PERFORMANCE AND IMPELLER FORCE OF TURBOPUMPS IN UNSTEADY OPERATION

H. Ohashi
University of Tokyo

H. Tsukamoto
Kyushu Institute of Technology

M. Kaneko
Mechanical Engineering Laboratory, MITI

H. Shoji
University of Tsukuba

Hydraulic performance of turbopumps and fluid force on their impellers in steady operating condition have been a center of pump study for long time. Limited information is available to the contrary on their behavior in unsteady condition. The present paper summarizes studies by the authors on the dynamic performance of turbopumps when the flow rate and/or rotational speed changes rapidly. Studies on the unsteady radial thrust of centrifugal impellers in whirling motion is also introduced.

1. Introduction

Hundreds of pumps are tested every day for their hydraulic performance and these data have been accumulated for long time. In these days pump design practice has so advanced, that design performance can be materialized with an utmost certainty. Analytical prediction of off-design performance, especially partial load performance, remains still of today's problem, but the estimation can be made with little difficulty from the past performance data of pumps with similar specific speed and design principle. The above situation refers, however, only to the case in which pumps operate in steady condition, that is, at constant flow rate and rotational speed.

In practice turbopumps operate often in unsteady condition. Typical example can be found in pumps in surging condition. When the pumping system is incorporated with some compliance, for instance air chamber or vapor cavity, and with some exciting mechanism, for instance positive gradient of flow to head curve, the system can be thrown into a severe self-exciting oscillation. For the precise analyses of these instabilities, it is necessary to know the dynamic character of every piping element including pumps. In the past analyses of POGO, a longitudinal structure/fluid coupled oscillation of liquid propellant rocket, the characteristics of turbopumps were assumed to be qusai-steady, since no information was available on their dynamic behavior [1].

The authors have been carrying the study on the dynamic characteristics of turbopump under various unsteady conditions. The present paper summarizes the result in the following three conditions:

1) Response of pressure rise, when the pump rotates at a constant speed and the flow rate fluctuates sinusoidally around its mean value [2].
2) Response of pressure rise, when the pump rotates at a constant speed and the flow rate increases or decreases rapidly by sudden opening or closure of discharge valve [3].

3) Response of pressure rise, when the pump is started from standstill to final speed quickly and the flow rate increases in accordance with the speeding up of the impeller [4].

There are of course many other aspects of unsteady characteristics. Intensive studies have been done for determining the response of cavitating inducers and impellers in terms of transfer matrices [5]. Pressure rise response of propellant feed pumps to fluctuating flow rate was measured by Shimura and Kamijo [6]. Transient performance of a centrifugal pump during quick start-up was reported also by Saito [7].

Hydraulic forces on impellers, usually divided into axial and radial thrust, are determining factors to the design of bearings and shaft strength. They are, however, indifferent to the rotordynamic instability of pump shaft. The very fluid force, which excites or damps the shaft vibration in bending mode, is unsteady non-synchronous lateral force on the impeller, when the center of the rotating shaft whirls on an orbit around its equilibrium position. Unsteady fluid force on oscillating impeller is therefore of great concern to rotor stability. In the last section of the present paper results on the lateral fluid forces on a whirling centrifugal impeller are introduced [8, 9].

For the torsional instability of pump shaft, the response of impeller torque to fluctuating rotational frequency is important. This aspect was studied by Imaichi and Tsujimoto [10]. As to the random fluctuation of radial thrust on non-whirling centrifugal impeller, which is induced either by the impeller/guide vane interaction or by the inherent flow turbulence in the impeller, several experimental results are available [11, 12]. Miyashiro et al. measured transient axial thrust of a two-stage vertical mixed-flow pump during start-up [13]. All these data are important for the rational estimation of random and transient loads to bearings and structural elements.

The study reported in the pesent paper was carried always in the frame of incompressible flow. The dynamic behavior of cavitating impellers and two-phase flow pumps is beyond the present scope.

2. Dynamic performance

2.1 Measured and true total head

Hydraulic performance of a turbopump at a constant rotational speed is expressed usually by a Q-H curve as illustrated in Fig. 1, where point 1 and 2 represent two operating conditions. When the discharge of the pump changes from Q_1 to Q_2 slowly, the instantaneous pressure rise of the pump varies obviously along with the steady Q-H curve. In the case of a quick change from Q_1 to Q_2, the time lag of the internal flow gives rise to a delay of the pressure rise of the pump, thus resulting in the deviation of dynamic Q-H curve from those in steady condition. The problem of dynamic peformance is hence to make clear; 1) the critical condition beyond which the quasi-steady assumption becomes inadequate and 2) the deviation of dynamic performance from quasi-steady one when the limit is surpassed.

In the case of unsteady operation special attention must be paid to the meaning of total head H of the pump. Total pump head is defined, for example by JIS B 0131, as the increase of total head from suction to delivery generated by the pumping action. In the case of steady flow rate, all total head is obviously generated by the pumping action of rotating impellers. In the case of unsteady flow rate, however, a part of the total head is caused by the inertia of water contained in impeller and casing. This part is called total head by conduit effect, H_c, and is calculated by the

equation

$$H_c = -(L_{eq}/gA_0)(dQ/dt) \qquad \text{.....(1)}$$

where A_0 is the reference cross sectional area, L_{eq} the equivalent length of the pump. In order to determine equivalent length, the flow passage of the pump from suction to delivery port must be transformed at first to a one-dimensional pipe with variable cross section A(s) as shown in Fig. 2, and then to an equivalent pipe of length L_{eq} with reference cross section A_0, where L_{eq} is given by the relation

$$L_{eq} = \int_{s=0}^{L} (A_0/A(s))\, ds \qquad \text{.....(2)}$$

The true total head by pumping action during unsteady operation, H , can be calculated from measured total head, H_m, and apparent total head by conduit effect, H_c, by

$$H = H_m - H_c \qquad \text{.....(3)}$$

Hereafter total head during unsteady operation is always meant for the true head calculated by the above procedure.

It is hardly possible to determine the equivalent length in an exact meaning. This is especially the case when the pump is equipped with a volute casing, in which the length of stream lines is different depending on the angular location of discharge into the volute. This fact implies that the equivalent length of volute is a function of fluctuation frequency in such manner that the higher the frequency, the shorter the equivalent length [14].

Equivalent length can be also estimated experimentally. For this purpose the flow rate is forced to oscillate by an external device while the pump shaft is kept standstill. The measured flow rate acceleration dQ/dt and total head H_c give rise to an equivalent length by Equation (1). This method involves also an uncertain factor, because the length of absolute stream line in the impeller is different depending on whether it rotates or stands still.

Total head by conduit effect, H_c, increases proportional to the fluctuation frequency and its uncertainty increases also accordingly. In higher frequency range where the dynamic performance of pumping action begins to deviate from steady one, H_c occupies predominant fraction of measured total head, H_m. Therefore, true total head, H , in highr frequency range can be estimated only with a considerable uncertainty.

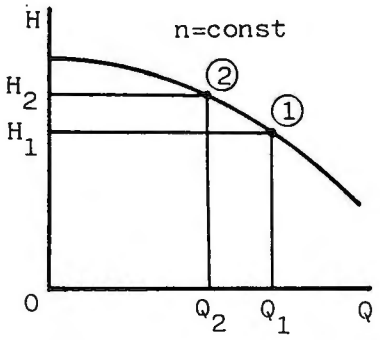

Fig. 1 Steady performance curve

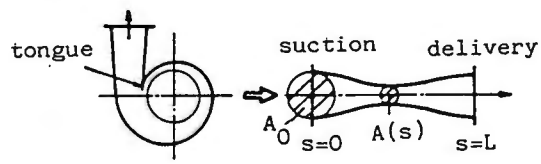

Fig. 2 Equivalent length

2.2 Mechanism of pressure rise lag

The mechanism why the pressure rise of an impeller cannot respond to the instantaneous flow condition and allows a certain time lag, is divided into three major factors:

1) Potential lag Potential lag is defined as the one which occurs even under the assumption of incompressible potential flow. Typical example can be seen in the lag of circulation and lift growth of an isolated airfoil when it changes its attack angle stepwise from zero to a finite value at t = 0. Fig. 3 shows the growth of circulation and lift calculated by Wagner [15], where U_∞ is uniform velocity, ℓ chord length, Γ_0 and L_0 asymptotic circulation and lift, respectively. As seen from this example, the time lag of potential flow in lift and circulation generation is about 2 in non-dimensional time unit, tU_∞/ℓ. The essential reason of this time lag consists in the fact that counter-vortices are shed from each trailing edge so as to suppress sudden change of airfoil circulation and it takes a definite time for them till they are carried so far away that they lose their suppressive effect.

From the above consideration it is clear that potential lag is proportional to chord length and inversely to flow velocity. In turbomachines potential lag is proportional to the period of rotation, or inversely to the rotational speed.

2) Viscous lag It requires a certain time for boundary layer to grow its thickness and eventually to develop into a separated region. Fig. 4 illustrates the evolution of pressure distribution around a circular cylinder after it starts moving suddenly from standstill. Parameter in the figure is displacement d normalized by cylinder radius. Immediately after the start the pressure distribution is very close to the one calculated by the potential theory and it proves that no separation region does exist at this moment. Only after the cylinder moves more than twice the diameter, the pressure distribution becomes similar to the steady one, which features a large separated region behind the cylinder. It is noteworthy that the lag time due to viscous effect is also about 2 x (representative length)/(representative velocity) as in the case of potential lag.

In the dynamic performance of turbopumps, potential lag seems to play an essential role, since the pressure rise of pumps is primarily achieved by lift of impeller vanes.

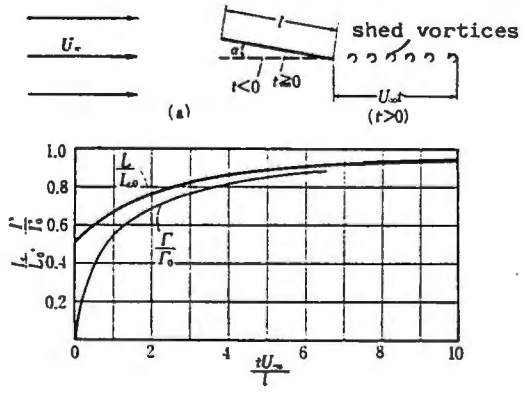

Fig. 3 Growth of circulation and lift

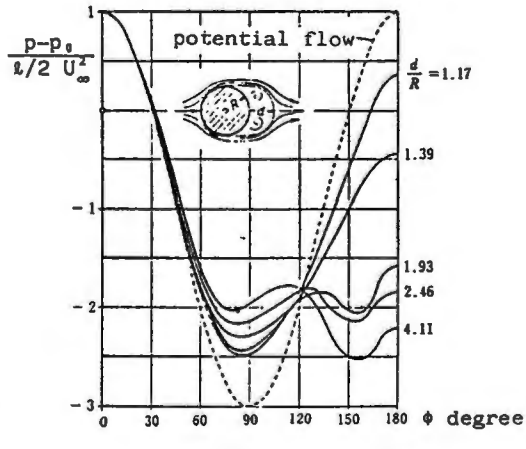

Fig. 4 Pressure distribution after sudden start

3) Compressibility lag In compressors handling compressible gas and even in pumps handling two-phase flow and cavitating flow, finite acoustic velocity or compliance causes definite lag. As stated in Introduction, no compressibility lag is taken into consideration in the present paper.

2.3 Response to fluctuating flow rate

Hydraulic performance of pump is considered, when it rotates at a constant speed and its flow rate Q fluctuates around its mean value Q_0 as $Q = Q_0 + \Delta Q \cos \omega t$, where ΔQ is the amplitude of flow fluctuation and $\omega=2\pi f$ is anglular fluctuation speed. In the case of very low fluctuation frequency, the quasi-steady assumption holds and the true total head of the pump, H, varies along with steady performance curve (cf. Fig. 1). Fig. 5 shows the relation between flow and total head change, where quasi-steady change of total head is indicated by broken line. As fluctuation frequency increases, dynamic total head indicated by solid line starts to deviate from steady one, and phase lag $\Delta\theta$ and decrease of head fluctuation, ΔH_{qs} to ΔH, take place. The dynamic response of pressure rise can therefore be expressed by the relation of $\Delta\theta$ and $\Delta H/\Delta H_{qs}$ to fluctuation frequency f.

Fig. 6 shows the arrangement of test setup schematically. A single-stage centrifugal pump with 50 mm suction diameter was used for the experiment. Flow fluctuation was induced by a pulsating piston attached to the delivery line, and was measured by a MHD flowmeter.

The results are summarized in Fig. 7. The phase lag $\Delta\theta$ in degree and

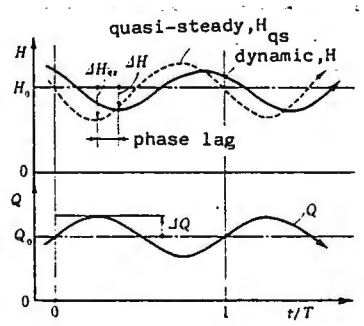

Fig. 5 Response of head to fluctuating flow

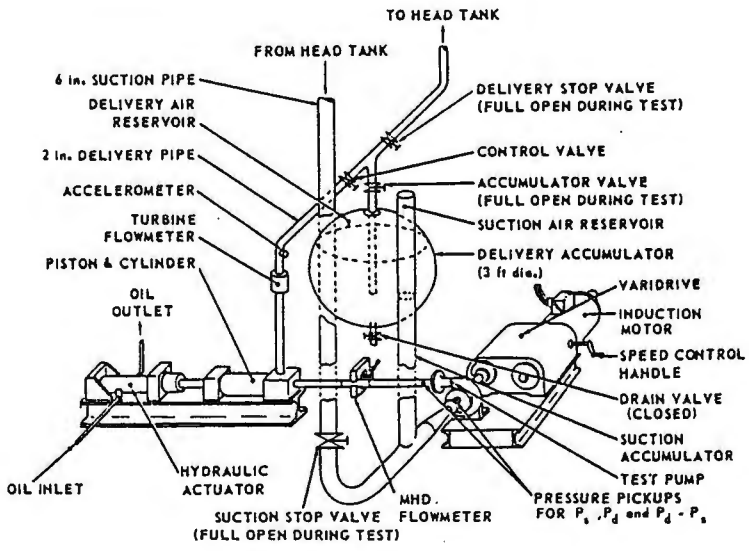

Fig. 6 Test setup

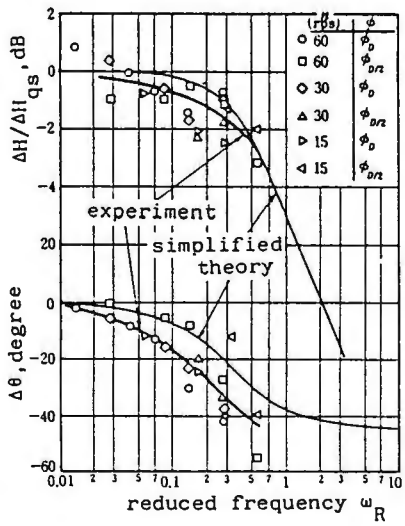

Fig. 7 Frequency response of total head

amplitude ratio $\Delta H/\Delta H_{qs}$ in decibel are plotted against non-dimensional frequency of impeller, $\omega_R = (\cos\lambda_R/N_R\phi)(f/n)$, where λ_R is stagger angle of impeller vanes, N_R number of impeller vanes, ϕ flow coefficient and n rotational speed. Data at three different rotational speeds and two flow coefficients (design and half-design flow) are plotted together. Thin solid lines in the figure indicate analytical result derived from unsteady flow around linear cascade. Pressure rise response depends of course on the geometries of both impeller and guide vane (rotor and stator). Simplified dynamic characteristics in the figure were obtained however by taking only the potential lag of impeller into consideration.

From the above mentioned result, followings can be interpreted:

1) The critical condition, beyond which quasi-steady assumption begins to fail, is expressed by $\omega_R \cong 0.1$. Critical fluctuation frequency f_{cr} can be calculated therefore by

$$f_{cr} \cong 0.1 \times (N_R\phi/\cos\lambda_R)\, n \qquad \text{.....(4)}$$

For a typical centrifugal impeller with $N_R = 8$, $\phi = 0.1$ and $\lambda_R = 25°$, critical frequency is about $f_{cr} \cong 0.1\ n$, and this can be used as a rule of thumb for common pumps.

2) When frequency exceeds critical one, phase lag increases and amplitude ratio of pressure rise response decreases as shown in Fig. 7. Let $\tilde{H}(s)$ the Laplace transformation of time-dependent total head variation $\tilde{H}(t) = H(t) - H_{mean}$, and $\tilde{H}_{qs}(s)$ that of $\tilde{H}_{qs}(t)$, the transfer function G(s) is defined by

$$G(s) \cong \tilde{H}(s) / \tilde{H}_{qs}(s).$$

Though the simplified dynamic response in Fig. 7 cannot be expressed by a simple transfer function in an exact sense, the relation can be approximated by $G(s) = 1/\sqrt{1+Ts}$, where time constant $T = 1/2\pi f_{cr}$. The maximum phase lag in theory is 45°. It is obvious that experimental result shows larger phase lag than theory predicts. The experimental response is better represented by a simple first order lag $G(s) = 1/(1+Ts)$.

The response of pressure rise to flow fluctuation $\tilde{Q}$ can be finally expressed by

$$\tilde{p}_d(s) - \tilde{p}_s(s) = G(s)\,[\tilde{p}_d(s) - \tilde{p}_s(s)]_{qs} = R_p\,\tilde{Q}(s)/(1+Ts) \qquad \text{...(5)}$$

where $\tilde{p}_d(s) - \tilde{p}_s(s)$ is Laplace transformation of pressure rise fluctuation, and $R_p = [\partial(p_d - p_s)/\partial Q]_{qs}$ is tangent of steady performance curve.

3) The above result applies only to the case of small fluctuation without cavity formation. If once cavitation occurs under severe pressure fluctuation, the linear relation between flow and pressure fluctuation deteriorates badly and fractional harmonics such as f/2, f/3 appears in the pressure fluctuation.

2.4 Response during quick opening and closure of discharge valve

In this section the response of pressure rise is reviewed when the flow rate increases rapidly from zero to a final value by quick opening of discharge valve, or decreases to zero by quick valve closure. The rotational speed is kept constant during the transient. A single-stage centrifugal pump with 50 mm suction diameter was used for the test. A ball valve actuated by an air cylinder executed on/off control of discharge, while another gate valve adjusted steady flow rate before and after the transient. From the recorded time histories of suction and delivery pressure, p_s and p_d, and flow rate Q, instantaneous head coefficient $\psi(t)$ and flow coefficient $\phi(t)$ are evaluated by

$$\psi(t) = H(t)/(u_2^2/2g), \quad \phi(t) = Q(t)/ d_2 b_2 u_2 \quad \text{.....(6)}$$

where H(t) is the true total head excluding conduit effect, d_2 outer diameter, b_2 exit width and $u_2=\pi d_2 n$ peripheral speed of impeller.

Fig. 8 shows transient characteristics during valve opening by loci of instantaneous operating point. Flow rate increases from zero to three different final values. In all cases the instantaneous head coefficient is obviously higher than those of steady characteristics. To the contrary, decreasing flow rate by quick valve closure results in less total head than steady performance assures, as seen from Fig. 9.

Analysis of unsteady potential flow during the transient leads to a theoretical transient response as shown in Fig. 10, in which theoretical and experimental characterisitcs during quick valve opening are plotted for comparison. Since potential theory cannot take account of flow losses, the absolute value of theoretical head is much higher than experimental one. However the deviation from the steady chasracteristics is quite similar in both cases and it suggests that potential lag plays a predominant role also in this case. The deviation from steady curve shows that the impeller circulation cannot decrease quick enough to keep pace with rapidly decreasing attack angle.

2.5 Response during quick start-up

When a pump is started from standstill by turning on of the driving motor, the shaft accelerates itself according to torque characteristics of the motor and moment of inertia of the rotating system, and reaches gradually its final speed. On the other hand, discharge flow rate increases also from zero. The acceleration of flow rate depends primarily on the

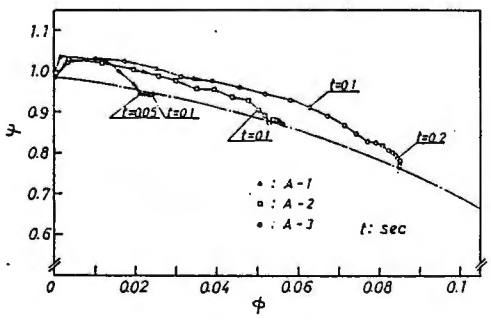

Fig. 8 Transient characteristics during valve opening

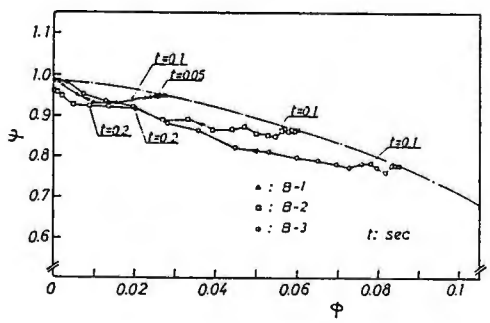

Fig. 9 Transient characteristics during valve closure

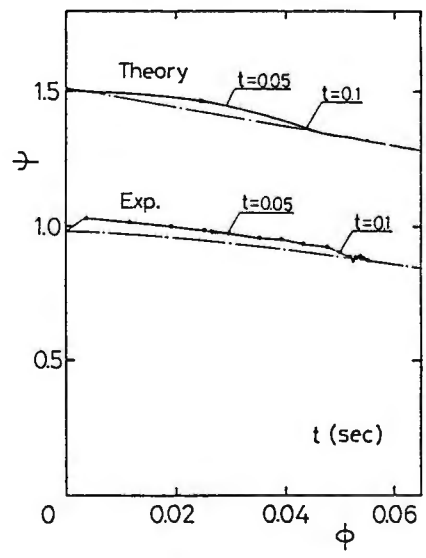

Fig. 10 Comparison between theory and experiment

inertial resistance of the piping system, that is, the total length of suction and delivery pipe. When the piping is very short, the flow rate increases along with rotaional speed with little delay, and reaches final discharge immediately after rotational speed gets to equilibrium. When the piping is very long, most of the pump pressure rise is allocated to accelerate the long water column and the flow rate continues to increase even after the shaft reaches its final speed. As explained in the above, the acceleration of rotational speed and flow rate are governed by independent factors. Therefore, the study of dynamic performance during quick start-up should make clear the response of pressure rise to arbitrarily given change of rotational speed and flow rate.

Experiment was carried by using a single-stage centrifugal pump with 50 mm suction diameter. In order to realize extremely high acceleration of rotaional speed, a magnetic friction clutch was used, which coupled pump shaft at rest directly with motor shaft in full rotation. For slower acceleration ususal switch-on start was also adopted. Acceleration time is represented by nominal time T_{na}, which is defined as the time to reach 63% of final speed N_f. The quickest acceleration time was T_{na} = 0.12 s. The discharge valve was so adjusted, that the final flow rate Q_f after the start-up tends to a desired operating point.

Fig. 11 (a) and (b) show the time histories of rotaional speed N, flow rate Q and true total head H at each instant after extremely quick (T_{na} = 0.12 s) and moderate (T_{na} = 0.68 s) start, respectively. The final flow rate was adjusted to design flow and the total length of suction and delivery piping was equivalent to 4.5 m long pipe with 40 mm inner diameter.

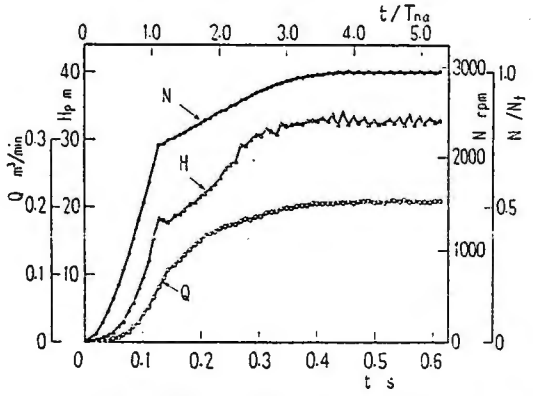

(a) Very high acceleration

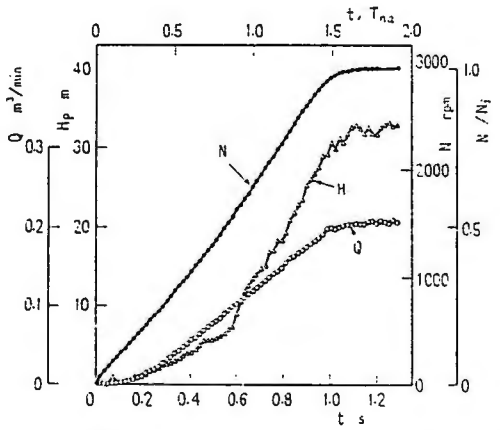

(b) Moderate acceleration

Fig. 11 Time histories during start-up

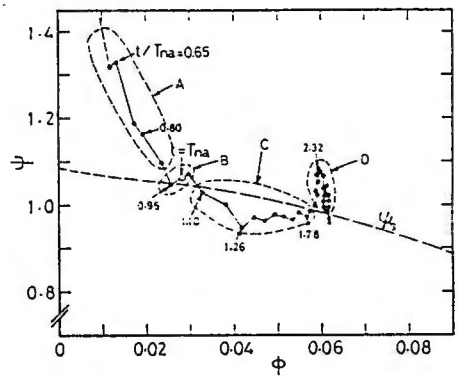

(a) Very high acceleration

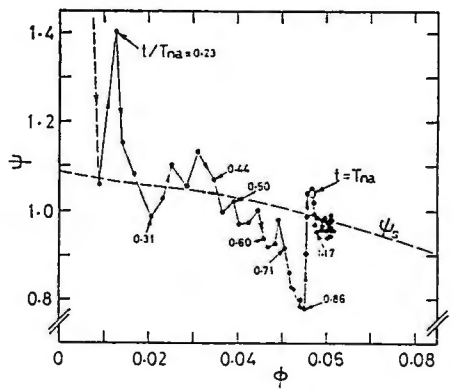

(b) Moderate acceleration

Fig. 12 Locus of operating point

The result of Fig. 11 can be converted into non-dimensional parameters such as instantaneous head and flow coefficient by Equation (6). In Fig. 12 (a) and (b) the locus of operating point during the start-up is plotted on the characteristics diagram, where broken line indicates steady characteristics curve. In the very early stage of the start-up (region A), the impeller produces larger head than the one expected from steady characteristiccs. This can be attributed partly to the impulsive pressure acting on quickly accelerating impeller vanes, and partly to the delay of separation.

In the intermediate stage (region C) head reduces to the contrary below the steady characteristics. This may be caused mainly by the potential lag of circulation growth (cf. 2.2). The shape of loci of operating points are not much different between (a) and (b). The essential difference due to acceleration time consists rather in the operating point at $t = T_{na}$. In the case of very quick start-up, cf. (a), the acceleration of water column cannot keep pace with rotaional speed and the flow coefficient at T_{na} remains still about half of its final value. In the case of slow and moderate acceleration, cf. (b), the delay of flow acceleration is less and the operating point comes close to the final point already in the latter stage of start-up.

Fig. 13 shows the comparison between analytical and experimental characteristics during quick start-up. Since the potential calculation cannot take the effect of flow losses into consideration, the absolute values of both results are again different. The comparison should be made in relation to the steady characteristics of each cases. It can be seen from the figure that the higher head in region A can be simulated well by potential theory, while the measured head reduction in region C is far larger than theory predicts.

From the dimensional analysis of start-up procedure an important parameter, $N_f T_{na}$, is introduced. This parameter is proportional to the total number of revolution till the impeller reaches final speed. The smaller the parameter, the stronger the effect of unsteadiness.

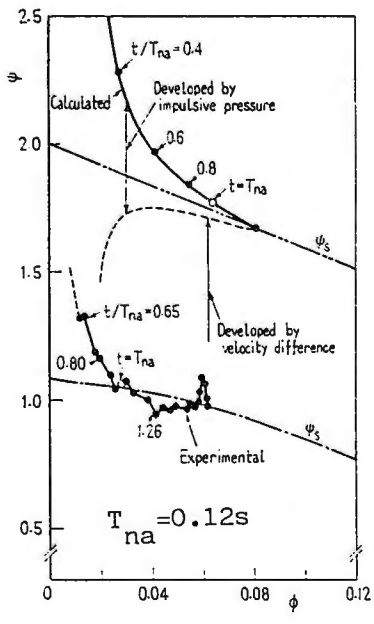

Fig. 13 Comparison between theory and experiment

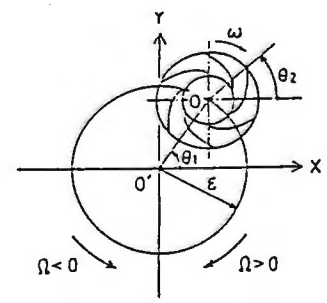

(a) Coordinates.

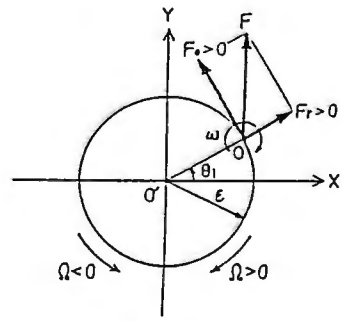

(b) Force vector

Fig. 14 Notations

3. Fluid force on whirling impeller

Fluid force on centrifugal impeller of vibrataing shaft is of great interest from rotordynamic point of view. This flow situation is so idealized that the impeller center O whirls on a circular orbit around a fixed center O' with an eccentric radius ε as shown in Fig. 14 (a). ω and Ω are angular speed of rotaion and whirl, and the latter Ω corresponds to the first damped natural frequency of shaft in bending mode (critical speed).

The fluid force on impeller, F, is called radial thrust in the case of non-whirling condition, but is called lateral force hereafter. As shown in Fig. 14 (b) lateral force is divided into two components; radial force F_r normal to whirling orbit and tangential force F_θ parallel to the orbit. Radial force works as bending force and is usually very small compared to the shaft stiffness. To the contrary tangential force parallel to the orbital motion feeds or extracts energy from the whirling system and plays a vital role to the stability of the rotor system.

In the present study these two forces, F_r and F_θ, were measured at various whirl speed ratio, Ω/ω, and flow coefficient ϕ and were compared with the analytical result.

Fig. 15 illustrates the whirling mechanism and installation of load cells for force measurement. Fig. 16 shows typical fluid force vectors and their scattering at 9 locations on the orbit, when the impeller whirls in vaneless diffuser. Radial and tangential forces are normalized by

$$f_r = \bar{F}_r/M\varepsilon\omega^2, \quad f_\theta = \bar{F}_\theta/M\varepsilon\omega^2 \qquad \text{.....(7)}$$

where M is the mass of working fluid displaced by the outer boundary of impeller, $M = \rho\pi r_2^2 b_2$, $\bar{F}_r$ and $\bar{F}_\theta$ are the force components averaged over the orbit.

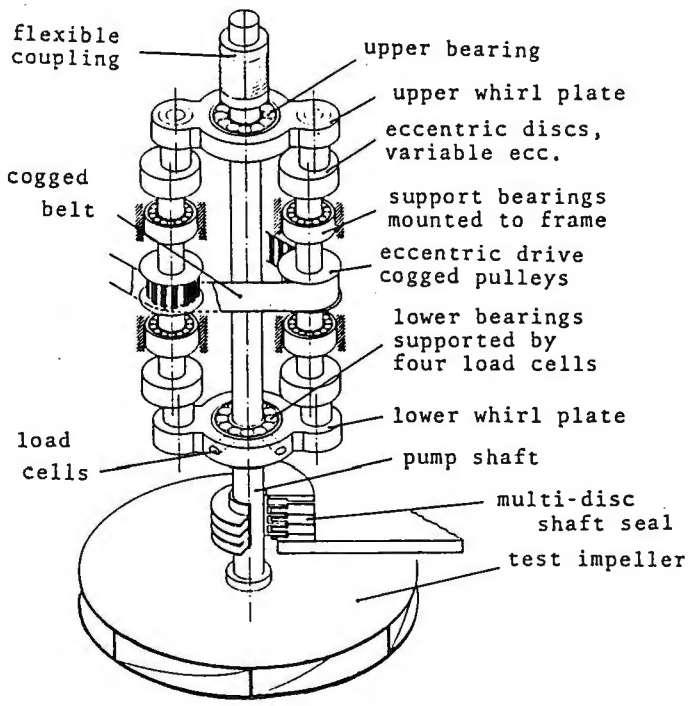

Fig. 15 Whirling mechanism

Fig. 17 shows the result, when a two-dimensional impeller with vane angle of 22° whirls in vaneless diffuser at various flow rate. The broken line indicates the analytical result at shock-free entry condition, $\phi=\phi_{sf}$. From this figure followings can be concluded:

1) Radial force acts outward and has a character of negative spring.
2) Tangential force exerts damping effect in most operating condition in positive and negative whirl.
3) At very low discharge near shut-off and at high supercritical rotational speed ($\omega>2\Omega$), tangential force does exert excitation to positive whirl, leading eventually to a self-excited oscillation called impeller whip.
4) In negative whirl larger damping can be expected than in positive whirl. Guide vanes around impeller augment damping effect to whirling motion.

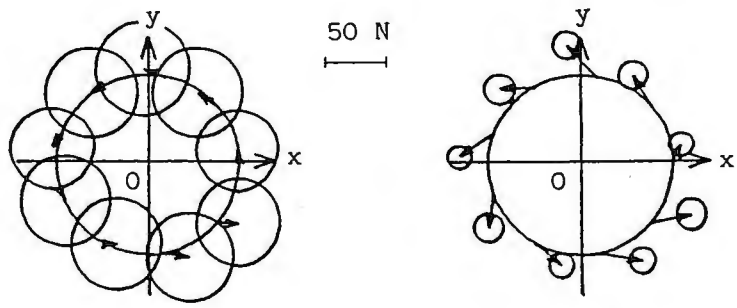

$\phi = 0$, $\Omega/\omega = 1.33$ $\phi = \phi_{sf}$, $\Omega/\omega = 1.33$

Fig. 16 Fluid force vectors and their scattering

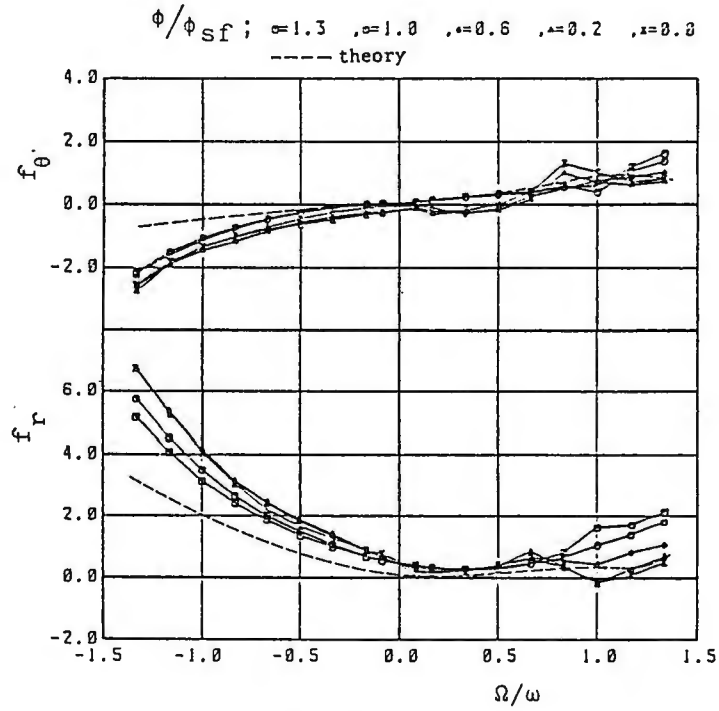

Fig. 17 Normalized fluid force in vaneless diffuser

It is further expected to accumulate data of whirling impeller forces for wide variety of impeller and volute geometries.

4. Conclusions

From wide aspects of dynamic behavior of turbopumps, dynamic performances at three different unsteady conditions are introduced on the basis of analytical and experimental study. The importance of fluid forces on whirling impeller is stressed and the result of recent study is referred.

Acknowledgement

This study was supported by Grant-in-Aid for Scientific Research by the Ministry of Education, Science and Culture. The authors appreciate the dedicated assistance to the experimental work by Messrs. H. Daigo, S. Yamamoto, S. Yanagisawa, K. Tomita, J. Hanawa, K. Kawakami and C. Kato.

References

[1] Fashbaugh, R.H. and Streeter, V.L., Resonance in Liquid Rocket Engine Systems, Trans. ASME, Ser. D, 87-4 (1965-12), 1011.

[2] Ohashi, H., Analytical and Experimental Study of Dynamic Characteristics of Turbopumps, NASA Technical Note TN D-4298 (1968-4).

[3] Kaneko, M. and Ohashi, H., Transient Characteristics of a Centrifugal Pump During Quick Change of Flow Rate, Trans. JSME, Ser. B, 48-426 (1982-2), 229 (in Japanese).

[4] Tsukamoto, H. and Ohashi, H., Transient Characteristics of a Centrifugal Pump During Starting Period, Trans. ASME, Journal of Fluids Engineering, 104-1 (1982-3), 6.

[5] Brennen, C. and Acosta, A.J., The Dynamic Transfer Functions for a Cavitating Inducer, Trans. ASME, Journal of Fluids Engineering, 98-2 (1976-6), 182.

[6] Shimura, T. and Kamijo, K., Dynamic Response of a Centrifugal Liquid Oxygen Rocket Pump, ASME, Paper 83-FE-24, Fluids Engineering Conf.(1983-6).

[7] Saito, S., The Transient Characteristics of a Pump During Start Up, Bulletin of JSME, 25-201 (1983-3), 372.

[8] Shoji, H. and Ohashi, H., Fluid Forces on Rotating Centrifugal Impeller with Whirling Motion, NASA Conference Publication 2133 (1980-5), 317.

[9] Ohashi, H. and Shoji, H., Lateral Fluid Forces Acting on a Whirling Centrifugal Impeller in Vaneless and Vaned Diffuser, 3rd Workshop on Rotordyn. Instability Problems (1984-5).

[10] Imaichi, K. and Tsujimoto, Y., Analysis of Unsteady Torque on a Two-Dimensional Radial Impeller, Trans. ASME, Journal of Fluids Engineering, 104-2 (1982-6), 228.

[11] Kanki, H. et al., Experimental Research on the Hydraulic Excitaion Force on the Pump Shaft, ASME, Paper 81-DET-71 (1981-9).

[12] Yamaguchi, Y. and Miura, S., Characteristics of Radial Force Fluctuations on Runners of Francis-Type Pump-Turbines. 1st Rep., Bulletin of JSME, 24-195 (1981-9), 1586.

[13] Miyashiro, H. and Takada, K., Axial Hydraulic Thrust Caused by Pump Starting, Trans. ASME, Ser. D, 94-3 (1972-9), 629.

[14] Anderson, D.A. et al., Response of Radial-Bladed Centrifugal Pump to Sinusoidal Disturbances for Non-Cavitating Flow, NASA TN D-6556 (1971-12).

[15] Wagner, W., Dynamischer Auftrieb von Tragfluegeln, ZAMM, 5-1 (1925-2), 17.